Ultranarrow-Linewidth Stimulated Brillouin Scattering with Fundamental Acoustic Waves

Wendao Xu,[1,a)] Maxime Zerbib,[2] Arjun Iyer,[1] Kien Phan Huy,[2,3] Jean-Charles Beugnot,[2] and William H. Renninger[1]

AFFILIATIONS

[1] Institute of Optics, University of Rochester, Rochester, NY 14627, USA
[2] Institut FEMTO-ST, Université Bourgogne Franche-Comté, CNRS UMR 6174, Besançon 25000, France
[3] SUPMICROTECH-ENSMM, Besançon 25000, France
[a)] **Author to whom correspondence should be addressed:** wxu21@ur.rochester.edu

ABSTRACT

Stimulated Brillouin scattering is a well-known nonlinear optical interaction valued for applications including narrow-linewidth lasers, phase conjugation, sensing, and rf-signal processing such as delay lines and filters. While interaction strength and linewidth directly affect device performance, most strongly interacting Brillouin systems have linewidths of many MHz, limited by the high frequency of the participating acoustic waves. By engineering Forward Inter-Modal Brillouin interactions to access the Fundamental Acoustic Modes (FIM-FAM), strong Brillouin coupling can be extended over a wide frequency range, including lower frequencies that support significantly narrower linewidths. In this work, sub-MHz Brillouin linewidths as narrow as 110 kHz are observed in tapered optical fibers with homogeneous waists. Tight confinement of both the optical and acoustic waves yields Brillouin gains over a thousand times higher than traditional backward Brillouin scattering in standard fibers, and a long waist and low-loss transitions enable a Brillouin interaction strength nearly a hundred times greater than prior taper-based FIM-FAM demonstrations. A specific radius and comprehensive polarization control suppress background scattering by over 40 dB relative to the signal. A comprehensive theoretical model is developed accounting for the dynamical behavior of optical and acoustic waves, reproducing qualitative behavior for several experimental configurations. In addition, the dependence of homogeneity of the linewidth is investigated and reveals a route towards further linewidth reduction by controlling phase-matched frequency variations throughout the waist. Extending strongly coupled Brillouin interactions to ultranarrow linewidths with a recipe for fabrication, detailed characterization techniques, and a comprehensive theoretical treatment will benefit high-performance Brillouin-based photonic applications.

1. INTRODUCTION

Stimulated Brillouin scattering efficiently couples light to an acoustic wave through electrostriction and radiation pressure forces. As one of the strongest nonlinear optical effects, Brillouin interactions have enabled important photonic technologies including narrow linewidth lasers [1–3], various microwave processing components[4–6], and powerful distributed temperature and strain sensors[7]. Compared to bulk materials or standard fibers, stronger interactions occur when the participating optical and acoustic fields are well confined and co-localized, as has demonstrated in several platforms, including nanoscale on-chip waveguides[8–12] and specialty optical fibers[13–16]. However, the linewidth of the interaction, which is a critical parameter for most applications such as microwave photonic filters, delay lines and storage devices[17–20], is much more challenging to improve and has been lower-limited to around 10 MHz in nearly all previous systems.

The Brillouin linewidth is determined by the acoustic dissipation of the system, which in addition to other loss mechanisms, is determined by intrinsic dissipation, which is proportional to the frequency of the interaction. Previous Brillouin platforms have been restricted in linewidth due to their high and fixed interaction frequencies. In the most common backward scattering arrangement in which the participating optical fields counter propagate, the acoustic frequency is fixed by momentum conservation (phase matching) to the GHz range. For example in strong coupling platforms including on-chip waveguides in chalcogenide[10] and suspended silicon[11], fiber tapers[21] and photonic crystal fibers[14], the linewidth is around 10 MHz. On the other hand, phase matching can be manipulated in the forward, optically co-propagating configuration with the use of higher-order guided acoustic modes. However, to achieve strong coupling, the waveguide cross-section generally needs to be small, which fixes the lowest available acoustic frequency (at cutoff) to also be in the GHz regime, as in suspended silicon and silicon nitride waveguides[8,9,11,12] and

photonic crystal fibers[16], resulting in MHz-level acoustic linewidths. In a notable exception, very high aspect ratio nanoweb waveguides can add flexibility with lower interaction frequencies and strong coupling, but the geometry is delicate and complex[13].

Recently, we have shown Brillouin waveguides in which co-propagating optical waves in distinct spatial modes can interact with much lower frequency acoustic waves in the fundamental acoustic modes with long lifetimes[22]. These Forward Inter-Modal interactions with the Fundamental Acoustic Modes (FIM-FAM) therefore are a promising candidate for ultranarrow linewidth Brillouin scattering. The frequencies of the fundamental acoustic modes do not have a cutoff which enables them to be much smaller than those of the higher-order modes. The specific frequency of interaction is determined by the relative propagation constants of the two participating optical modes. Previously, FIM-FAM has been demonstrated with large Brillouin gain in a few-mode fiber taper at 134 MHz with long acoustic lifetimes (~2 μs). However, because axial geometric variations combined with the long acoustic lifetimes introduces self-interference of phonons generated within different axial segments of the taper, the spectral response is complex with an effective broadening much more than the intrinsically supported dissipation linewidth. In addition, these devices were not desirable for single-frequency applications because the waveguide supported several high-order optical modes resulting in multiple closely spaced resonances. Finally, the Brillouin interaction strength was limited by high insertion losses (99%) and a short waist length (<10 mm). Applications requiring narrow linewidth responses will typically require low insertion loss, a clean single frequency response, and large coupling strength, which each involve distinct theoretical and technical challenges to achieve.

Here we demonstrate strong FIM-FAM interactions featuring a single-resonance with a narrow linewidth (~100kHz) response and low insertion loss, in a long waist (~100 mm) highly homogeneous (< 2% variation) few-mode fiber taper with minimal guided optical modes, and near adiabatically varying transition regions. The combination of narrow linewidths due to high homogeneity, a long waist region, and low insertion loss enables a strong interaction strength of 0.115, which is ~90 times larger than in previous designs[22]. The narrow waist of the taper restricts the number of guided modes, which along with comprehensive polarization control, enables a relative contrast of the desired peak of over 40 dB compared to other measurable Brillouin resonances. A full theoretical model is developed for the measured FIM-FAM interactions, which in addition to previous treatments, adds a phase mismatch term accounting to inter-modal dispersion, which is essential for agreement with several unique experimental arrangements of the participating optical tones. Finally, the multi-variable effect of geometric variation on the FIM-FAM frequency and, in turn, linewidth, is explored and a pathway toward additional Brillouin linewidth narrowing is described. A flexible stimulated Brillouin interaction that is strong and capable of very narrow linewidths promises a new performance regime for photonic applications such as filters, delay lines, lasers and sensors.

2. DESIGN, FABRICATION, AND CHARACTERIZATION

Forward inter-modal Brillouin interactions (FIM) enable optical-mode-tunable phase-matching of acoustic waves with small wavevectors, and the fundamental acoustic modes (FAM) have no cutoff frequency and accessible wave-vectors and frequencies that extend to zero. Combining FIM access of FAM, therefore, enables FIM-FAM to access frequencies over a wide range including lower frequencies with much longer intrinsic lifetimes[22]. The aim of this study is to translate this longer lifetime into a correspondingly narrow response linewidth through suitable device design (Fig. 1a).

FIM-FAM interactions occur between a fundamental acoustic wave with frequency Ω and wavevector q, and two co-propagating optical fields guided by separate spatial modes, a pump field with frequency ω_p and wavevector β_P and either a Stokes or anti-Stokes field with frequency ω_S or ω_{AS} and wavevector β_S or $\beta_{AS.}$ The optical wavevector, β, is given by the free-space wavelength, λ, and the effective refractive index of the guiding optical mode, $n_{eff,}$ as $\beta = 2\pi n_{eff}/\lambda$. The Stokes process occurs when its frequency is smaller than the pump frequency and the anti-Stokes process occurs when it is larger. The direction of acoustic wave propagation is determined by the modes chosen for the optical signals through phase-matching such that for the Stokes (anti-Stokes) process, for example, if the pump is in an optical mode with a larger effective refractive index, n_{eff}, than the Stokes (anti-Stokes), $\beta_P = \beta_S + q$ ($\beta_P = \beta_{AS} + q$), and the acoustic wave must travel in the same (opposite) direction as the light (Fig. 1b). In contrast, when n_{eff} of the Stokes (anti-Stokes) is larger, $\beta_P = \beta_S - q$ ($\beta_P = \beta_{AS} - q$), and the acoustic wave must travel in the opposite (same) direction from the light. Since the speed of light is orders of magnitude faster than that of acoustic waves, the frequency shifts of the Stokes and anti-Stokes components relative to the pump are negligible in the optical domain and both the Stokes and anti-Stokes processes interact with the same acoustic wave. The coupling strength of the interaction is determined by the cross-sectional overlap between forces produced by the two interacting optical

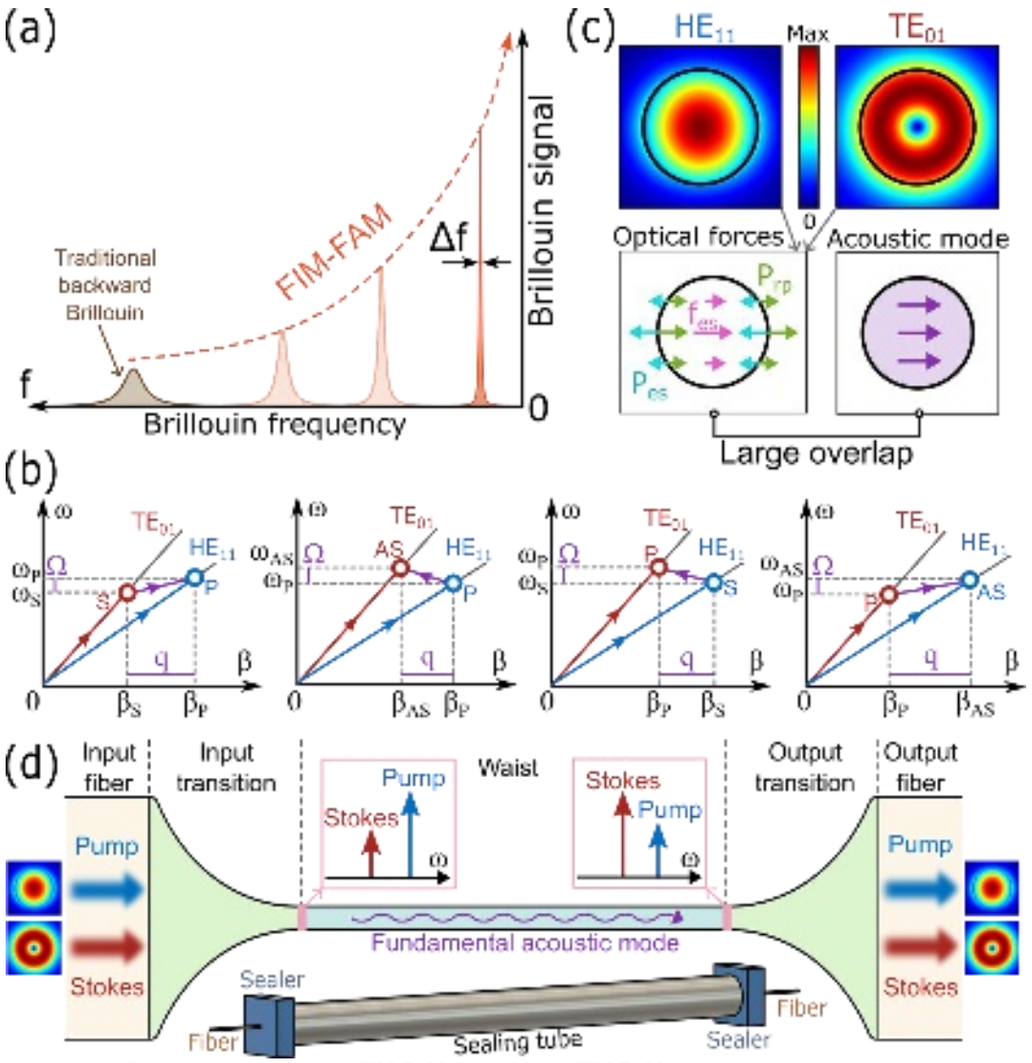

Fig. 1. Narrow-linewidth Brillouin scattering through FIM-FAM interactions. a) FIM-FAM enables access to lower frequency acoustic waves than traditional Brillouin interactions, enabling narrower linewidths and larger coupling than traditional backward Brillouin interactions in silica waveguides. b) Illustrative phase-matching and energy-conservation diagrams for four cases, showing the pump (P) propagating in either the fundamental or higher-order optical mode, with the Stokes (S) or anti-Stokes (AS) sidebands propagating in the corresponding other mode. While the associated acoustic mode is nearly identical in each case, the acoustic wavevectors appear different for illustrative clarity because of the scale adjustments needed to compensate for the difference between the optical and acoustic frequencies. Here one can see that the acoustic wave co-propagates with light for the Stokes process with the pump in the fundamental mode (first subfigure) and for the anti-Stokes process with the anti-Stokes in the fundamental mode (fourth subfigure), and the acoustic wave counter-propagates with light for the other two cases (second and third subfigures). c) FIM-FAM coupling is calculated by simulating the two participating optical modes (top) to generate the optical force (bottom left including bulk electrostriction, f_{es}, surface electrostriction, P_{es}, and radiation pressure, P_{rp}) and overlapping with the simulated displacement field for the acoustic field (bottom right). d) The taper design regions with an example interaction configuration overlaid. The pump and Stokes are coupled into the uniform waist region through the input transition region, from the input standard two-mode fiber. The forward-propagating acoustic wave in the fundamental mode is excited at the waist region, and the pump energy is partially transferred to the Stokes sideband via FIM-FAM. The pump and Stokes are coupled out of the waist region into the output fiber, through the output transition region. Inset: The taper sample is securely packaged within a sealing tube.

modes and the fundamental acoustic wave[23,24] (Fig. 1c). The optical forces can be calculated by numerically solving for the two participating optical modes and including contributions from electrostriction inside and around the surface of the waveguide as well as radiation pressure on waveguide surfaces. The acoustic frequency of the fundamental acoustic mode is then determined by the phase-matched acoustic wavevector given by the difference of the effective refractive indices between the two optical modes. Finally, an overlap integral of the displacement field associated with this acoustic mode is integrated with the optical forces over the cross-section to find the FIM-FAM gain.

A fiber taper is designed to support a single-frequency FIM-FAM response with large coupling strength and an ultranarrow linewidth. A few-mode fiber taper consists of a waist region with a small radius between two transition regions with slowly varying radii used to couple light into the waist from and out of the waist to input and output few-mode fibers (Fig. 1d). As described previously[22], an efficient FIM-FAM interaction occurs in the waist region between the fundamental optical mode, one of the higher-order optical modes, and the fundamental flexural acoustic mode. Different properties of the taper, fabrication process, and measurement procedure must be advanced and optimized to achieve simultaneous narrow linewidths, large coupling strength, and a single-frequency response.

Achieving narrow linewidths first requires a long intrinsic acoustic lifetime, which is a function of the bulk material dissipation, and scattering losses on the taper surface. As demonstrated previously[22], the intrinsic lifetime for the low frequency acoustic modes associated with FIM-FAM in tapers is long and on the order of microseconds. The challenge is to translate this long lifetime into a narrow linewidth response considering fabrication imperfections which introduce axial variations along the taper waist. As has been discussed for backward and forward intra-modal Brillouin systems with short-lived phonons[25], as well as for FIM-FAM systems with long-lived phonons[22], geometric inhomogeneity in Brillouin-active waveguides introduce frequency shifts to the nominal Brillouin frequency, which translates to a spectral broadening of the FIM-FAM linewidth. To minimize axial variations of the FIM-FAM frequency, the waist region should be as homogeneous as possible. This can be achieved by designing the waist radius to remain uniform by optimizing the fabrication process to reduce deviations introduced during production.

Achieving strong coupling requires optimization of the Brillouin interaction strength, given by $G_B P_p L$, where G_B is the Brillouin gain coefficient, P_p is the optical power of the pump, and L is the interaction length. Each of these factors can be separately maximized to achieve the largest possible interaction in the fiber taper. G_B is enhanced by the tight confinement of the optical and acoustic modes from the silica-air boundary around the taper waist. G_B is also inversely proportional to the acoustic linewidth, which means that achieving a narrow linewidth will also directly enhance the gain of the system. P_P can be increased directly, but assuming a fixed pump source, the pump can be used more efficiently if a higher fraction of power is coupled into the modes of interest. This translates to increasing the transmission efficiency of the optical mode guiding the pump through the input transition region. It will also help similarly for the net response signal to increase the transmission of the other mode guiding the signal through the output transition region. Reducing the coupling loss in the transition regions requires a careful design for adiabatic transitions which requires long transition regions (see supplementary material S1 for a full analysis). In this study, the input and output transition regions are designed to be symmetric with low loss for all the fundamental and higher-order optical modes with a 35 mm axial length for each region. Finally, L should be as long as possible given the constraints of the fabrication system. A waist region as long as 100 mm is designed, constrained practically by gravity-induced sagging at the center and the maximum length of the fabrication setup including the waist and the transition regions.

Achieving a single frequency response requires optical and acoustic mode isolation through careful design of the taper waist, and appropriate polarization control in the experimental setup, respectively. The radius of the taper waist needs to be large enough to support two modes for FIM-FAM, but small enough to not support additional modes which would introduce additional resonances, since each mode pair can in principle generate a FIM-FAM response. The number of FIM-FAM resonances, therefore, is determined by the number of modes in the taper waist, which is determined by the normalized frequency, $V = \frac{2\pi r}{\lambda}\sqrt{n_{co}^2 - n_{cl}^2}$, where r is the waist radius, $n_{co} = 1.444$ is the refractive index of the fused silica, and $n_{cl} = 1$ is the index of the air cladding. The stepped-index input fiber is designed to only support two modes, the fundamental, LP_{01}, and the higher-order, LP_{11}, mode. In the input transition region, light in the LP_{01} mode couples into the fundamental mode of the waist, HE_{11}, and light in the LP_{11} mode couples into a combination of the higher-order modes in the waist, TE_{01}, TM_{01} and HE_{21} (Fig. 1c). In our previous design[22], the waist radius of 830 nm allowed all three higher-order optical modes to be guided, resulting in three distinct FIM-FAM resonances which were difficult to suppress sufficiently to achieve an effective single-frequency response. To reduce the available mode pairs, the waist is reduced to allow the minimum of two higher-order modes, TE_{01} and TM_{01}, by reducing the V-parameter below the cutoff for guidance for the HE_{21} mode which will dissipate into the air by the end of the input transition region[26]. The targeted normalized frequency V is therefore between 2.405 and 2.756, which corresponds to a design waist radius that is between 570nm and 650 nm, with a nominal target design of 600 nm to accommodate potential fabrication uncertainties. With this design target, only two resonances are accessible, and a single resonance can be selected preferentially by mode control in the mode-selective coupler through polarization, as described in the next section.

The fiber taper is fabricated at the Institut FEMTO-ST with a heat-brush technique, which is well known for its versatility in achieving customized fiber taper profiles[27,28]. It can generate fiber tapers with long and homogeneous waists, as well as long transition regions with profiles targeting high optical transmissions. Through this process, a hydrogen-oxygen flame heats the center of the taper while two translation stages holding the fiber ends shape the taper profile by moving along the trajectories calculated with an adapted version of an algorithm previously used to target ultra-low-loss in single mode fiber tapers[29]. The measured taper sample is physically realized after several iterations of optimization, refining the designed local angles of the transition regions along the entire length and fine-tuning the stage movement parameters governing the practical trajectory creation. This careful optimization ensured a smooth axial evolution of the taper radius, resulting in a highly precise and well-engineered taper profile. More detailed information on this advanced taper fabrication process targeting high-performance FIM-FAM can be found in supplementary material S1. For international transportation to the University of Rochester for FIM-FAM spectroscopy, the taper samples are stretched slightly in the axial direction to maintain the complete taper profile and glued at the fiber sections on either end on top of a specifically designed 3D-printed support. The sample with the bottom support is then placed into a stainless-steel tube and sealed on both ends with two 3D-printed sealers to fix the relative movements between the sealing tube and the taper sample (Fig. 1c inset).

After fabrication, the fiber tapers are characterized and analyzed with a variety of techniques before FIM-FAM spectroscopy described in the next section. First, optical backscattering reflectometry reveals that the lengths of the waist region and the transition regions are close to the designed values of 100 mm and 35 mm, respectively. Backward Brillouin spectroscopy reveals a waist radius of around 615 nm, which is comfortably within the design target window for guiding only the fundamental (HE_{11}), and two higher order modes, TE_{01} and TM_{01} (see supplementary material S2). With transmission measurements from input to output fibers, the optical transmission of the fundamental, HE_{11}, mode is measured to be ~82%, and the transmissions of the TE_{01} and TM_{01} mode are measured to be > 3.6% and > 4.0% respectively. While interpretation of the HE_{11} measurement is straight-forward because the input fiber, taper waist, and output fiber all have a single symmetric mode, interpretation of the higher-order mode transmission is more difficult. In this case, light from the input fiber LP_{11} mode can couple spatially to the TE_{01}, TM_{01}, and HE_{21} modes in the waist. Because the TE_{01} and TM_{01} modes result in measurable FIM-FAM responses, one can be minimized to extinction through polarization control as described in the next section. However, because the amount of light that couples into the non-guided HE_{21} mode cannot be measured directly and is unaccounted for by simple transmission measurement, the actual light in the higher-order modes of interest will be slightly higher and the estimated power in the higher-order mode should therefore be considered a lower bound. Nonetheless, the measured transmissions, while not yet at their maximum allowed (recipe for future improvements in supplementary material S11), are about 4 times larger than in our previous report[22] and lead to (a comparable enhancement in signal) at least a 2x enhancement in $G_B P_p L$ as described in section 4 below. Forward intramodal Brillouin measurements of the fundamental optical mode reveal a maximum fluctuation of the waist radius of only ~2.5% around the average measured radius, corresponding to an exceptional nm-level of homogeneity ideal for the investigation of narrow linewidth responses (see supplementary material S3). Finally, the FIM-FAM gain and response frequencies can be calculated using the measured waist radius. From optical simulations, the three effective mode indices are found to be 1.24 (HE_{11}), 1.03 (TE_{01}) and 1.01 (TM_{01}). Then, the numerical simulations of the acoustic fields are performed using typical mechanical properties of the fused silica, with the phase-matched acoustic wavevectors for interactions between HE_{11} and TE_{01} and between HE_{11} and TM_{01}. The phase-matched FIM-FAM frequencies are found to be ~189 MHz for the TE_{01} resonance and ~210 MHz for the TM_{01} resonance. The optical forces are calculated using the simulated the electric fields and integrated with the simulated acoustic displacement field over the cross-section. The flexural acoustic mode couples strongly with the participating optical modes giving a gain of 506 $W^{-1}m^{-1}$ for the TE_{01} and 361 $W^{-1}m^{-1}$ for the TM_{01} resonance. For ideal homogeneity and intrinsically-limited acoustic loss, these gain values with the measured improvements in P_p and L would enable an incredible $G_B P_p L$ product near 1 for both modes. In practice, the actual value will depend on how the narrow the linewidth is based on inhomogeneity and the complex Brillouin interactions.

3. EXPERIMENTAL SETUP

FIM-FAM is measured with a phonon-mediated four-wave mixing spectroscopy approach building from previous sensitive Brillouin spectroscopy techniques[22,30,31] (Fig. 2). With the four-wave mixing technique, two optical drive tones generate an acoustic wave in the FIM-FAM device, and a third tone at a distinct frequency probes the driven acoustic wave which scatters to generate a fourth tone that is sensitively measured with heterodyne detection. The first acoustic drive, drive 1 ($\omega_{d1} = \omega_c + \omega_1$), is generated with a null-biased intensity modulator modulating carrier frequency, ω_c, with frequency ω_1, with three fiber Bragg grating (FBG) filters used to suppress the unwanted modulator's lower frequency sideband (ω_f). Drive 1 is then input into port 1 of a mode selective coupler (MSC) which couples to the

fundamental mode (HE_{11}) of the fiber taper, which is fusion spliced to the MSC's output two-mode fiber. For the other two input tones, an acousto-optical modulator (AOM) with a center frequency Δ is used to upshift the carrier from the laser frequency ($\omega_{c2} = \omega_c + \Delta$). The AOM prevents the frequency of the residual unwanted modulator sideband, ω_f, from overlapping with the Stokes signal frequency, and, along with additional electrical feedback loops, enables stabilization of the relative frequencies between the optical tones of interest to within 1 Hz, as implemented previously[22]. Drive 2 ($\omega_{d2} = \omega_c + \omega_2 + \Delta$) and the probe ($\omega_{pr} = \omega_c - \omega_2 + \Delta$) are then generated from the frequency-shifted carrier (ω_{c2}) with another null-biased intensity modulator driven at frequency ω_2 ($\omega_2 < \omega_1$), and both are input into port 2 of the MSC which couples to the higher-order TE_{01} and TM_{01} modes of the fiber taper. When the frequency difference of two acoustic drives matches the FIM-FAM resonant frequency of the taper ($\omega_{d1} - \omega_{d2} = \Omega$), a fourth tone, the anti-Stokes sideband (it would be Stokes if $\omega_2 > \omega_1$ instead - see supplementary material S7 for a detailed discussion of variations) of the probe, scatters into the fundamental optical mode from the fundamental flexural acoustic wave generated by the drive tones. The resultant anti-Stokes FIM-FAM signal (as well as residual drive 1) in the fundamental mode efficiently couples into the single mode of the receiving fiber collimator, while both the drive 2 and probe in the higher-order modes are strongly rejected due to their orthogonal mode symmetry. After two FBG filters rejecting residual light from the drive tones, the signal couples into a photodetector with an additional local oscillator derived from the carrier frequency, ω_c, to generate the RF signal for a signal analyzer. Due to the bias drift and the non-ideal performance of the null-biased intensity modulator located before port 2 of the MSC, a small residual amount of carrier leakage can occur. This leakage allows a portion of the optical carrier to enter the few-mode taper, accompanying both drive 2 and the probe. Since this leaked carrier is spectrally separated from the optical tones

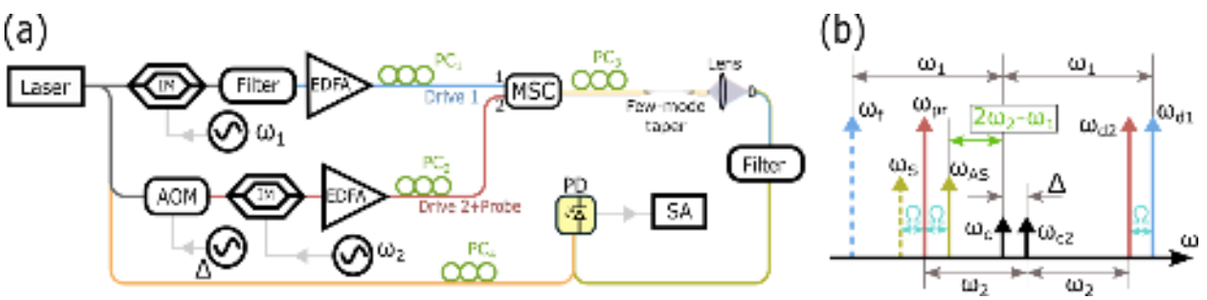

Fig. 2 a) The FIM-FAM measurement setup and b) corresponding frequency relationships between the optical tones as described in the text. With $\omega_{d1} > \omega_{d2}$ in this case the phase-matched anti-Stokes sideband of the probe is generated instead if the Stokes sideband. IM: intensity modulator (null-biased); EDFA, erbium-doped fiber amplifier; AOM, acousto-optic modulator; PC. Polarization controller; MSC, mode selective coupler; PD, photodetector; SA, electrical spectrum analyzer.

participating in the FIM-FAM, it does not contribute to the interaction. It is then filtered out by the FBGs after the collimator before the heterodyne detection. To acquire the FIM-FAM spectral response, the acoustic drive frequency, $\omega_{d1} - \omega_{d2} = \omega_1 - \omega_2 - \Delta$, with ω_1 fixed is swept by sweeping ω_2 through the resonance frequency, Ω, while tracking the RF signal at the corresponding beat frequency ($2\omega_2 - \omega_1$) (Fig. 2b).

Four polarization controllers are placed throughout the setup (see Fig. 2a) to optimize mode coupling and the measurement strength. To obtain a single-resonance FIM-FAM response, light in the higher order mode (LP_{11}) of the MSC's output two-mode fiber must couple into only one higher-order mode of the fiber taper (i.e. only TE_{01} or only TM_{01}). The coupling ratio between the LP_{11} and the taper modes (TE_{01} and TM_{01}) is determined by the polarization of the single-mode fibers input to the MSC as well as that of the LP_{11} mode on the output of the MSC. To suppress the unwanted higher-order mode, therefore, manual polarization controllers are used to control the polarization at the input of port 2 of the MSC (PC_2) [32,33] and on the MSC output fiber (PC_3). The adjustment on the polarization controller PC_3 also influences the polarization of the fundamental HE_{11} mode in the taper. A polarization controller on the local oscillator fiber (PC_4) is used to maximize the beat signal on the spectrum analyzer through aligning the local oscillator to the polarization of the FIM-FAM response signal. To selectively excite a single FIM-FAM resonance using the HE_{11} and TE_{01} modes, the other resonance modes can be suppressed by maximizing the RF power of the desired response at the photodetector through adjustments of the polarization controllers PC_2, PC_3 and PC_4. In order to calibrate the transmission loss of the beat signal from the detector to the spectrum analyzer, the residual probe light that leaks into the detector, originating from the finite mode rejection of the collimator and the mode cross-coupling throughout the whole taper, is utilized. The leaked probe is aligned to the FIM-FAM signal at the collimator by adjusting the polarization of the drive 1 and FIM-FAM signal with PC_1. Since the FIM-FAM gain coefficient is insensitive to the polarization state of the HE_{11} mode, the FIM-FAM signal strength remains unchanged during this

process. By measuring the strength of the beat signal between the local oscillator and the leaked probe on the spectrum analyzer, along with the optical power of the leaked probe at the detector, the RF signal loss from the detector to the spectrum analyzer can be determined and then used to correct for the beat signal strength between the FIM-FAM signal and the local oscillator. A single FIM-FAM resonance driven by the HE_{11} and TM_{01} can alternatively be measured by minimizing the response from FIM-FAM driven by the HE_{11} and TE_{01} modes in a similar way.

4. RESULTS

Optimized measurements of the FIM-FAM device reveal high-contrast nearly single-peaked responses with linewidths as narrow as 110kHz and a Brillouin interaction strength that is nearly two orders of magnitude greater than in previous devices (Fig. 3). The anti-Stokes sideband is observed because it is phase-matched by ensuring that drive 1 is at a higher frequency than drive 2 (Fig. 3 blue and orange). In contrast, light at the Stokes frequency in this condition is > 45 dB weaker (nonzero due to weak modal cross-coupling in the taper), confirming the non-reciprocity the interaction (Fig. 3 purple). A spectral response is also absent when the drive tones are off, as expected (Fig. 3 green). The anti-Stokes resonances between the fundamental mode HE_{11} and the two high-order modes TE_{01} and TM_{01} are observed at 203 MHz and 228 MHz, respectively, which is within 10% of the predicted frequencies, deviating slightly due to the uncertainty of the mechanical properties of the material and the axial strain in the physical sample introduced in fabrication and packaging. With optimized polarization adjustments described in the previous section, a single response corresponding to the TE_{01} mode is realized with > 40 dB contrast compared to the remainder of the spectrum, which includes the response from the TM_{01} mode, the Kerr four-wave-mixing background and other (non-FIM-FAM) Brillouin responses from the fiber taper and the connected two-mode fiber (Fig. 3a). Alternatively, a single-peaked response from the TM_{01} mode can be optimized for with >30 dB contrast compared to the remainder of the spectrum (Fig. 3b).

With sufficient spectral resolution, each resonance exhibits complex spectral structure owing to the small residual axial inhomogeneity of the fiber taper waist (Fig. 3c). The 3-dB linewidth of the primary peak from the TE_{01} resonance is 110 kHz, which is much narrower compared to the previous FIM-FAM taper sample[22] and other types of established high-gain Brillouin systems. The 3-dB linewidth of the major peak from the TM_{01} resonance is similar but broader at 240 kHz due to subtleties in the phonon self-interference effect and the frequency dependence of FIM-FAM as a function of the local taper radius, described in detail later in this section.

The FIM-FAM interaction strength, given by $G_B P_p L$, can be determined for the dominant peaks in the spectrum. In four-wave mixing spectroscopy the FIM-FAM signal power is given by $P_{sig-peak} = \frac{G_B^2 L^2}{4} P_{d1} P_{d2} P_{pr}$, where L is the FIM-FAM active waveguide length, P_{d1} is the power of the drive 1, P_{d2} is the power of the drive 2, and P_{pr} is the power of the probe. The interaction strength per unit power, $G_B L$, in units of W^{-1} then describes the coupling strength per unit pump power of the entire device. With this we find that the major peak from the TE_{01} (TM_{01}) resonance has an $G_B L$ of 5.75 W^{-1} (1.51 W^{-1}), both more than an order of magnitude larger than the previous FIM-FAM taper devices because their enhanced length and homogeneity. When used with a simple two-tone pump-probe configuration, the signal would be in the fundamental mode because it has less loss than the higher-order mode, and because the transmission of the higher order mode is improved in this device by ~4 times (2 times for each transition), the maximum FIM-FAM pump power at the waist is then at least two times larger than before. Overall, therefore, the current taper sample enables > 90 times larger interaction strength ($G_B P_p L$) than in the previous taper-based FIM-FAM platform, a major advance for photonic applications. While the peak gain is high, it is still at least five times lower than what it would be if the spectrum had strictly one clean peak, as is assumed in the interaction strength estimates from Section 2, for example. This is because, although mostly weak, the overall spectral response extends a bandwidth of around 5 MHz, which is more than ten times the linewidth of the primary peak. This broad bandwidth in the FIM-FAM response stems from the dependence of the FIM-FAM frequency on the taper radius, which varies slightly in the waist region. The complex spectral distribution that extends this bandwidth is determined by phonon self-interference, which occurs in systems with acoustic waves that live long enough to interfere with other acoustic waves generated in distinct axial locations along the fiber[22].

The FIM-FAM spectrum is broadened because the phase-matched frequency has a strong dependence on the taper waist radius, which varies due to fabrication imperfections. Because the difference in effective optical indices of the fundamental and higher-order optical modes as well as the phase velocity of the fundamental acoustic wave depend on the waist radius, the FIM-FAM frequency is a complex function of the axial waist variation. Using a refractive index of 1.444 for the fused silica and the optical wavelength at 1550 nm, the effective indices of the guided optical modes can be numerically simulated with finite element solvers for any waist radius, and the phase-matched acoustic

wavevector can then be used with the density (2203 kg/m^3), the pressure-wave speed (5903 m/s), and the shear-wave speed (3709 m/s) to calculate the FIM-FAM frequency. The FIM-FAM frequency is calculated vs. waist radius for the possible interactions between the HE_{11} mode and three different higher-order modes, TE_{01}, TM_{01} and HE_{21} (Fig. 3d). Each interaction has an inhomogeneity-insensitive radius at which the frequency is independent of the radius, which for interactions with the TE_{01}, TM_{01} and HE_{21} modes are calculated as 609 nm (r_1),707 nm (r_2) and 679 nm (r_3), respectively. These values are expected to vary slightly because of the < 10% variation for the measured frequency vs prediction. The dependence in (Fig. 3d) is corrected by a corresponding vertical shift such that it aligns with the measured frequencies at 615 nm radius, but a complete model would require the exact mechanical properties of the material and the axial strain profile of the taper. Importantly, the axial inhomogeneity of the radius will broaden the FIM-FAM spectral response in proportion to the slope of this frequency dependence on radius. Since the frequency variation for interactions with the TE_{01} resonance is predicted to be less than that from the TM_{01} resonance (comparing the slopes in Fig. 3d) the corresponding linewidth from the TE_{01} resonance should be narrower, which is consistent

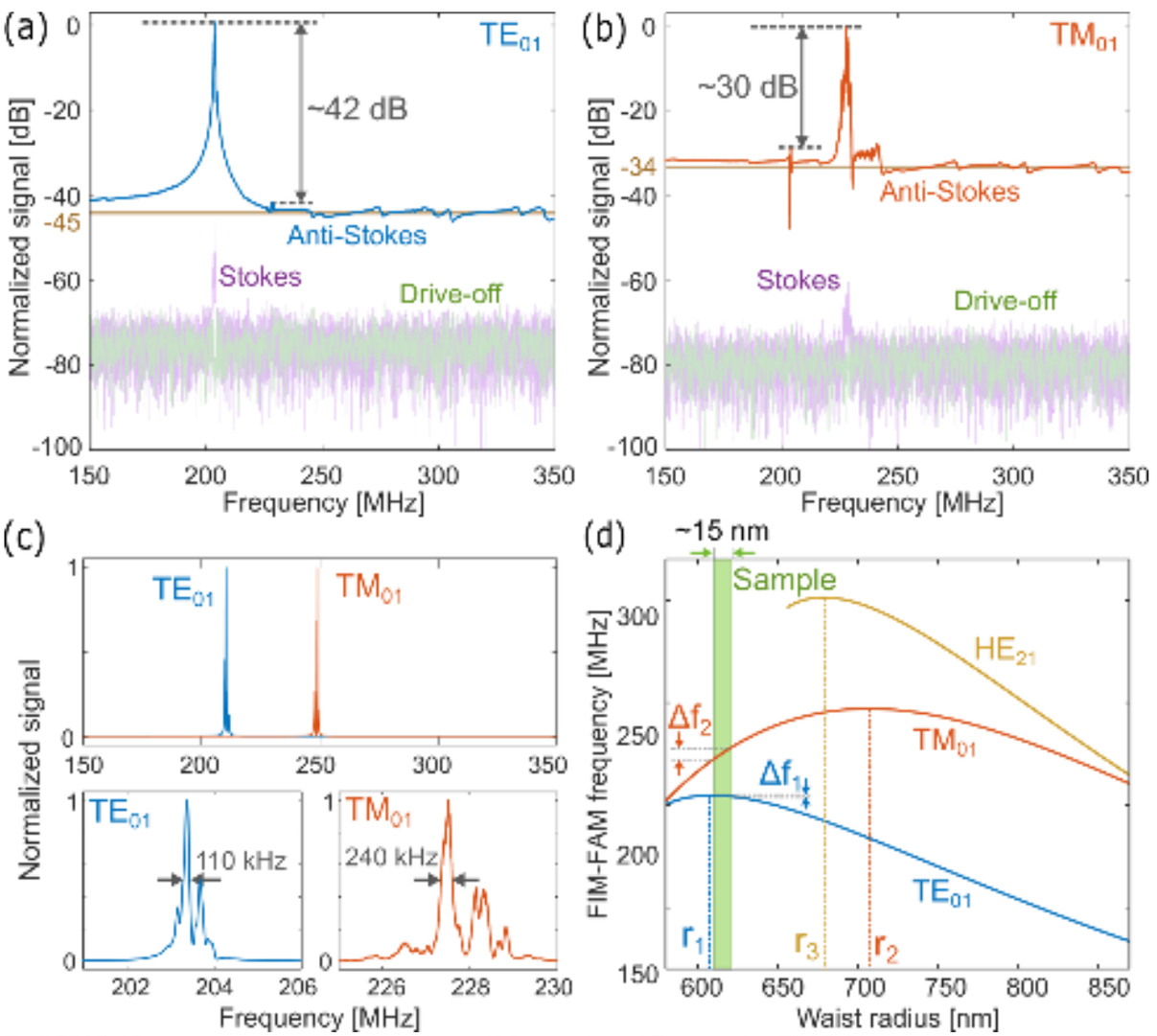

Fig. 3 FIM-FAM measurement results and homogeneity sensitivity analysis. a-b) The normalized FIM-FAM response signal measured from 150 MHz - 350 MHz obtained by polarization optimizing for either the TE_{01} (blue) of TM_{01} (orange) resonances, with the non-phase matched Stokes response (purple) and undriven (green) response shown for comparison. The TE_{01}(TM_{01}) mode is maximized to ~45 dB (~30 dB) higher than the background. c) The normalized TE_{01} (blue) of TM_{01} (orange) resonances on a linear scale with enough detail to resolve the narrow linewidth of the peak of 110 kHz and 240 kHz. d) Calculated FIM-FAM frequency dependence on the waist radius showing the values where each resonance is maximized and the frequency changes minimally with variation (r_1 for TE_{01}, r_2 for TM_{01}, r_3 for HE_{21}). The measured sample with ~15nm radius fluctuation (green bar) has an average radius closer to the inhomogeneity-insensitive radius of the TE_{01} resonance at r_1, compared to the calculated that of the TM_{01} resonance, leading to smaller broadening for the TE_{01} interaction (Δf_1) that for the TM_{01} interaction (Δf_2).

with the experimental results in Fig. 3c (see also supplementary material S5). Therefore, to further improve the linewidth toward intrinsic dissipation levels, the fabrication could be designed with the same fixed inhomogeneity to finely sample the mean radius with the aim of reaching the radius where the frequency varies the least. In addition, environmental (e.g. temperature) controls can be introduced around the taper to compensate for any post-fabrication drifts from this peak value.

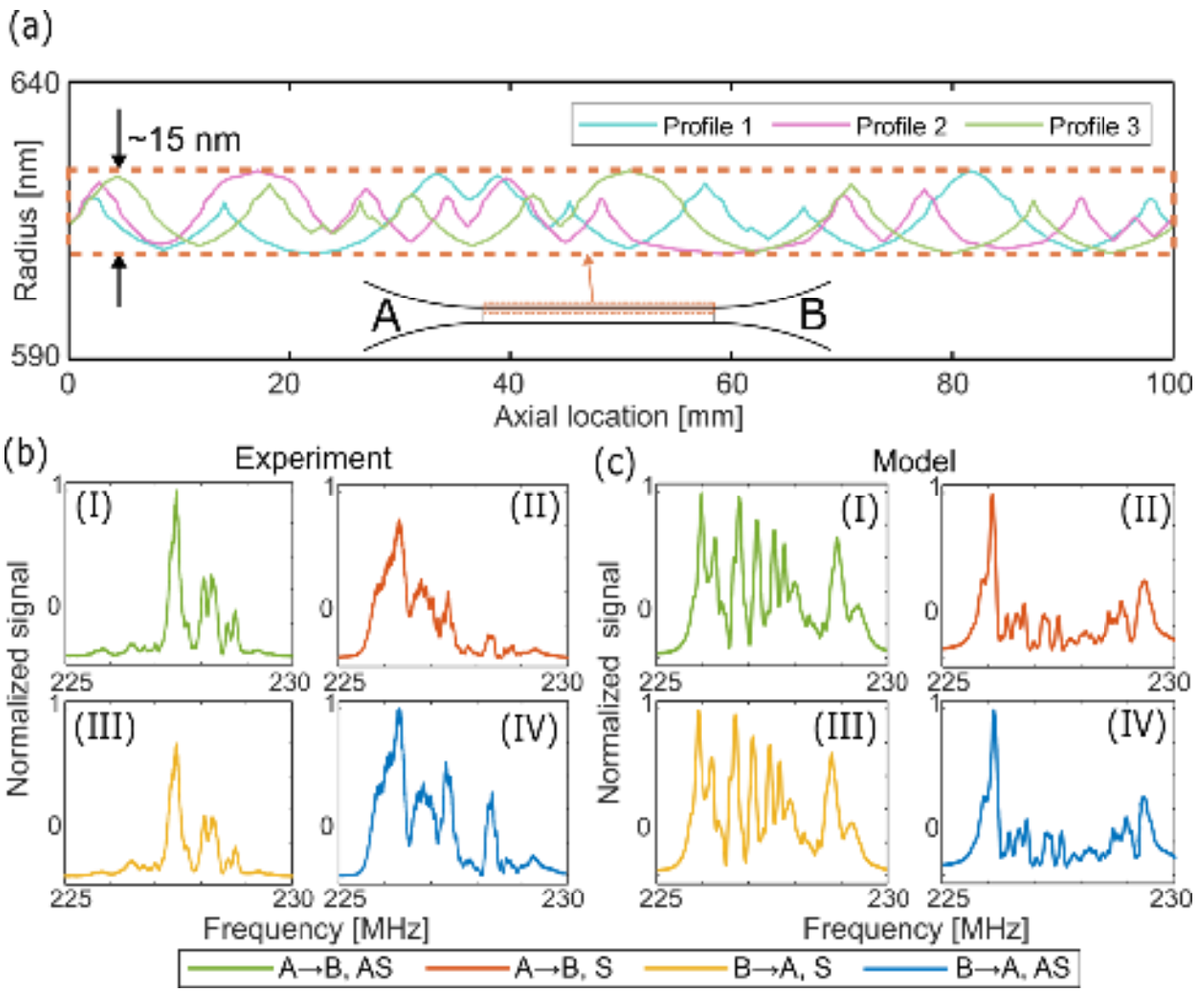

Fig. 4 Theoretical model for FIM-FAM dynamics including phonon self-interference with qualitative comparison to measurments. a) Three hypothetical waist profiles with the same radius histogram within ~15 nm over the 100-mm waist with ends A and B. b) Measured TM_{01} response for four different configurations: from A to B, driving the anti-Stokes (I) and (II) Stokes sidebands, and from B to A driving the (III) Stokes and (IV) anti-Stokes sideband. c) The corresponding predicted responses using hypothetical profile 1 from a) showing the similarity between (I) and (III) and (II) and (IV) and dissimilarity between (I) and (II) and (I) and (IV) as observed in the experiments in b).

To further analyze the spectral characteristics of the FIM-FAM response, we generalize the phonon self-interference model developed previously[22] to include the effects of modal dispersion to qualitatively predict the behavior of FIM-FAM in the near-homogeneous limit under several different operation conditions. We then use this complete model with an estimated geometric profile to predict the spectrally integrated response strength for comparison with measurements. In the absence of a non-destructive method to accurately measure the taper waist profile with nm-level resolution, we first develop an algorithm for generating physically plausible estimations for the taper profile. This can be done by modeling the experimental spectra with a traditional simplified inhomogeneous broadening model that neglects the long decay length of the acoustic wave [25] (see supplementary material S6). Through this technique the measured frequencies and amplitudes correspond to the radii and prominence in the taper waist, which can be represented by a histogram. While this histogram does not correspond to a unique profile, we select three plausible profiles based on this information from the measured TM_{01} resonance (Fig. 4a) for analysis with

the theoretical model. To obtain enough information for vetting the major qualitative inputs and behaviors of the model, the FIM-FAM spectra of both resonances are measured in four different configurations (Fig. 4b). Labeling the two physical ends of the taper waist region as A and B (Fig. 4a inset), the FIM-FAM spectra shown previously in Fig. 3 are measured by launching the optical tones from A to B, and placing drive 2 at a lower frequency compared to drive 1 to drive the anti-Stokes sideband as the signal (Fig. 4b-I). Alternatively, drive 2 can be put at a higher frequency compared to the drive 1 to drive the Stokes sideband (Fig. 4b-II). These two spectra can also be measured in the opposite direction, from B to A (Fig. 4b-III for the Stokes spectrum, Fig. 4b-IV for the anti-Stokes spectrum). Further details on the spectral phenomena observed in different configurations can be found in supplementary material S7. The model developed previously[22] does correctly predict the similarity between spectra measured with both opposite physical directions (e.g. from A → B to B ← A or vice versa) and opposite sidebands (e.g. Stokes to anti-Stokes or vice versa), i.e. between Fig. 4b-I and Fig. 4b-III, and Fig. 4b-II and Fig. 4b-IV. However, the dissimilarities between the spectra measured between either just opposite phase-matched sidebands or just opposite physical directions, e.g. between Fig. 4b-I and II, or Fig. 4b-I and IV, fail to be modelled without including the additional effects of modal dispersion (see supplementary material S8). In four-wave-mixing spectroscopy there is a ~20 GHz frequency separation between the drives and the probe and signal so the unwanted frequencies can be easily spectral filtered. However, as a result, the dispersion of both optical modes leads to a slight difference between the phase-matched acoustic wavevector of the acoustic drives, and the phase-matched acoustic wavevector of the probe-signal pair. This phase-mismatch is added to the signal generation process with the driven acoustic wave similar to that in the theoretical model of the Kerr four-wave-mixing process[34]. With this addition, the complete model can accurately account for the similarities and dissimilarities in Fig. 4 (see supplementary material S8) for each of the hypothetical waist profiles with profile 1 for the TM_{01} resonance shown in Fig. 4c. I.e. the spectra are now different between Fig. 4c-I and Fig. 4c-II, as well as between Fig. 4c-III and Fig. 4c-IV. As the phase mismatch is proportional to the frequency separation between the drives-pair and the probe-signal pair, its effect will reduce as it decreases (see supplementary material S9) and vanish when it approaches zero as it would if the interaction were a 2-tone instead of a 4-tone process. In this case, in the absence of the dispersion-introduced phase mismatch, the FIM-FAM responses remain identical regardless of the selected phase-matched Brillouin sidebands or the orientation of the device.

With a theoretical model for the FIM-FAM spectra, the total response across the spectrum can also be compared to predictions. Since G_B is proportional to the square of the overlap between optical forces and acoustic displacement and is inversely proportional to the square of the FIM-FAM frequency[23] the simulated G_B can be first corrected by substituting the measured FIM-FAM frequencies, which results in G_{OM} of 439 $W^{-1}m^{-1}$ for the TE_{01} resonance and 306 $W^{-1}m^{-1}$ for the TM_{01} resonance. To characterize the gain over the full response, the FIM-FAM spectral response is integrated as $P_{sig-tot} = \int_0^\infty P_{sig}(\Omega)\, d\Omega$, where $P_{sig}(\Omega)$ is the power spectral density of the FIM-FAM spectra. The total experimental response, $P_{sig-tot}^{exp}$, is directly obtained from the measured spectra and the total theoretical response, $P_{sig-tot}^{th}$, can be calculated from the modeled spectra generated using the modified phonon self-interference model, incorporating three hypothetical waist profiles and the calculated gain G_B. For profiles 1, 2 and 3, the total modeled TE_{01} responses are 1.9 times, 4.0 times and 3.6 times of the measured TE_{01} total response, respectively. Meanwhile, the modeled TM_{01} total responses are 1.2 times, 91% and 65% of the corresponding measured TM_{01} total response. While there is qualitative agreement between the experimental and theoretical responses, the discrepancies are largely attributed to uncertainty in the actual waist profile and intermodal dispersion (as discussed in supplementary material S9). Compared to the TE_{01} resonance, the TM_{01} resonance shows closer alignment between the experimental and modeled total integrated responses which may be related to the fact that the hypothetical waist profiles were derived from the measured TM_{01} spectra.

5. DISCUSSION

In this work, we have demonstrated FIM-FAM interactions in fiber tapers with 3-dB linewidths from 100 to 300 kHz, with the narrowest linewidth of 110 kHz. Ultranarrow linewidth Brillouin-based devices can improve the performance of applications such as microwave photonic filters, which directly benefit from the narrowest available response[19,35]. The ultranarrow Brillouin linewidth achieved here can be attributed to the combination of the low acoustic frequencies accessed by FIM-FAM, exceptional geometric homogeneity from a novel fabrication technique, and an average radius corresponding to an interaction frequency that changes minimally with small radius variations. The lowest measured linewidth is close to the 100 kHz predicted for the intrinsic dissipation of the system given the FIM-FAM frequency of ~200 MHz and a quality factor of 2000 ± 200 as extracted from previous measurements[22]. Further narrowing of the linewidth will require both reducing the intrinsic acoustic linewidth and minimizing the spectral broadening as a function of geometric variation. The intrinsic acoustic linewidth depends on the both the

resonance frequency and the propagation loss of the acoustic wave. The frequencies of the three observed FIM-FAM resonances, currently around 200 MHz, can be reduced by increasing the taper radius, which decreases the accessible acoustic wavevectors. Furthermore, a larger taper radius enables the guidance of higher-order optical modes with larger mode numbers which can provide an additional degree of freedom for tuning the FIM-FAM frequency through use of different pairs of optical modes which would phase match to different acoustic frequencies. However, increasing the taper waist radius would come at the cost of undesired mode cross-talk and a weaker FIM-FAM interaction strength. The acoustic loss could also be improved by reducing the ambient temperature of the waveguide[36] and refining the fabrication process to reduce the intrinsic and surface scattering loss of the traveling acoustic wave. The quality factor of the mediated acoustic wave is comparable to that of the higher-order modes in standard optical fibers with near-ideal surfaces and smaller acoustic surface-to-volume ratios, which suggests that surface roughness in the fiber taper does not contribute significantly to the observed acoustic dissipation compared to intrinsic loss mechanisms[37,38]. On the other hand, to avoid spectral broadening, the radius should be designed at a value such that variations produce minimal changes to the FIM-FAM frequency, as described in Section 4.

The combination of narrow linewidths due to high homogeneity, a long waist region, and low insertion loss enables a strong coupling strength (defined by $G_B P_p L$), for the TE_{01} mode of 0.115 with an input power of 100 mW, which is ~90 times larger than in our previous design[22]. This can be improved first with improved fabrication homogeneity, or a better design radius with less sensitivity to the inhomogeneity such that the linewidth is reduced. The total interaction strength can also be improved with increased power obtained from improvement in the optical transmission of the higher-order optical modes at the input transition region. The adiabaticity of fiber taper transition regions for dissipation of the optical modes has been extensively investigated[39,40]. To demonstrate an increase in transmission for the high-order modes, another taper sample sharing a similar homogeneous waist profile is designed and fabricated with smaller local angles in the transition regions, at the cost of elongated transition regions and a shorter waist length at 35 mm (see supplementary material S4). This led to increased high-order mode transmission of over 15%. Further transmission improvements are limited by the total length limitation of the translation stages and the requirement that the length be long enough of sufficient interaction. The tradeoff between the transition angle and waist length is constrained by the current design of the transition regions, which were originally optimized for low-loss single-mode fiber tapers. By refining the design of the transition profiles, taper adiabaticity can be enhanced without increasing the axial length of the transition regions (see supplementary material S11). Taper samples with improved transition regions showing > 50% transmission for the higher-order optical modes have been fabricated and used to demonstrate sub-MHz linewidth microwave photonic bandpass filters based on the interactions demonstrated in the present work, to be described elsewhere. For a 100% homogeneous and fully adiabatic (unity optical transmission) few-mode taper with the same 100 mm waist length, a FIM-FAM interaction strength as high as 4.39 is expected, which means ~40 times more improvement from the present work is available through these techniques. In the few-mode taper, it is challenging to further reduce the number of guided optical modes while still maintaining the multi-mode guidance of the waveguide, since the two higher-order TE_{01} and TM_{01} modes share the same cutoff radius. While the unwanted optical mode has been largely suppressed with comprehensive input polarization controls, unwanted cross-coupling will be challenging to eliminate completely. This, combined with the challenge for further frequency reductions through smaller mode index differences, motivates investigations beyond few-mode fiber tapers for photonic platforms with flexible design spaces for high-confinement transverse waveguide structures that support strong FIM-FAM with low-frequency and single-resonance responses.

The quantitative deviations of the modelled FIM-FAM spectra from the measured results originate from several factors including the deviation of the optical and acoustic properties used in the numerical simulations compared their physical values; the uncertainty on the acoustic quality factor that is obfuscated from spectral measurements by phonon self-interference; the unknown axial strain imposed during the fabrication and packaging; the unknown fraction of optical power that couples into the unguided HE_{21} taper mode from the mode-selective coupler; and most importantly, the uncertainty of the actual finely resolved geometry of the taper waist profile. The nm-level variations of the waist radius profile is challenging to measure over the entire waist length with sufficient transverse resolution even with scanning electron microscopy, which is destructive and would prevent further experimental investigations on the same sample [21,41]. Although non-destructive time-domain-based Brillouin characterization methods[42–44] could potentially extract part of the axial profile of the fiber taper, further exploration is needed to ensure very high transverse and axial resolutions needed here, which are at the nm and mm levels, respectively. Given the theoretical complexity of the evolution dynamics for the driven acoustic fields and the FIM-FAM optical response fields, it will be challenging to directly extract the waist profile from the measured spectra. Furthermore, forward calculations from hypothetical geometries to spectral prediction require extensive computation which complicates testing many hypothetical profiles to best match the measured spectra. In addition, a fraction of power from the LP_{11} fiber mode can potentially couple

into the unguided HE_{21} waist mode of the taper, which adds uncertainty to the remaining fraction of drive 2 and probe power that participate in the FIM-FAM interaction. Finally, small changes in the transverse azimuthal symmetry after the fabrication could potentially modify of theoretical treatment presented. Despite these challenges, properties are most desirable for applications including the peak signal response, linewidth, and spectral isolation, are unambiguously determined here, and the theoretical models and analysis developed in this report provide the insights and design guidelines needed for further advances in performance for FIM-FAM-based photonic technologies. On the other hand, further progress in the development theoretical tools for back-calculating the specific geometry from the complex measured spectrum leads to new applications, such as an optical approach to geometric spectroscopy through FIM-FAM.

6. CONCLUSION

Strong single-resonance FIM-FAM Brillouin interactions are demonstrated with linewidths as narrow as 110 kHz in low-loss, long and homogeneous-waisted fiber tapers. Ultranarrow linewidths are attributed to the combination of low acoustic frequencies, exceptional geometric homogeneity, and an average taper radius with minimal sensitivity to variation. A single resonance is isolated by engineering the taper waist to guide fewer optical modes and by precise polarization control to couple to fewer optical modes. The Brillouin interaction strength measured on resonance is ~90 times larger than in previous studies of FIM-FAM in fiber tapers due to the combination of the long, homogeneous waist and the low loss from the transition regions. Despite the challenges of measuring the exact taper waist profile, a comprehensive theoretical model is developed that accounts for measurements from several different experimental configurations. Future reductions in the linewidth are predicted by designing waveguides to operate at a geometry that has minimum sensitivity of the complex dependence of the FIM-FAM frequency to variations in the waist radius. Moreover, the conditions for adiabatic taper transitions for few-mode fibers are determined for design with minimal optical loss and corresponding maximum FIM-FAM response. The ultranarrow linewidths demonstrated in this work hold clear promise for a new performance regime for Brillouin-based photonic applications.

SUPPLEMENTARY MATERIAL

The supplementary material provides additional information on the design, fabrication, and characterization of the few-mode fiber taper, an in-depth derivation and analysis of the phase-mismatch-modified FIM-FAM theoretical model, and design guidelines for enhancing the performance of future FIM-FAM devices.

ACKNOWLEDGEMENTS

This work was supported by the National Science Foundation (Grant No. ECCS-1943658), the Office of Naval Research (Grant No. N000142312704 and N000142412012), the EIPHI Graduate School (Grant No. ANR-17-EURE-0002) and the Conseil régional de Bourgogne-Franche-Comté.

AUTHOR DECLARATIONS

Conflict of interest

The authors have no conflicts to disclose.

DATA AVAILABILITY

The data that support the findings of this study are available from the corresponding author upon reasonable request.

References

[1] N.T. Otterstrom, R.O. Behunin, E.A. Kittlaus, Z. Wang, and P.T. Rakich, "A silicon Brillouin laser," Science (80-.). **360**(6393), 1113–1116 (2018).
[2] K. Liu, J. Wang, N. Chauhan, M.W. Harrington, K.D. Nelson, and D.J. Blumenthal, "Integrated photonic molecule Brillouin laser with a high-power sub-100-mHz fundamental linewidth," Opt. Lett. **49**(1), 45 (2024).
[3] G. Bashan, H.H. Diamandi, Y. London, K. Sharma, K. Shemer, E. Zehavi, and A. Zadok, "Forward stimulated Brillouin scattering and opto-mechanical non-reciprocity in standard polarization maintaining fibres," Light Sci. Appl. **10**(1), 1–14 (2021).
[4] M.K. Varun, A. Mishra, and R. Pant, "Microwave photonics applications of stimulated Brillouin scattering," J. Opt. **24**(6), 063002 (2022).
[5] J. Li, H. Lee, and K.J. Vahala, "Microwave synthesizer using an on-chip Brillouin oscillator," Nat. Commun. **4**(1), 1–7 (2013).
[6] R. Pant, D. Marpaung, I. V. Kabakova, B. Morrison, C.G. Poulton, and B.J. Eggleton, "On-chip stimulated brillouin scattering for microwave signal processing and generation," Laser Photonics Rev. **8**(5), 653–666 (2014).
[7] A. Motil, A. Bergman, and M. Tur, "[INVITED] State of the art of Brillouin fiber-optic distributed sensing," Opt. Laser Technol. **78**, 81–103 (2016).
[8] R. Van Laer, B. Kuyken, D. Van Thourhout, and R. Baets, "Interaction between light and highly confined hypersound in a silicon photonic nanowire," Nat. Photonics **9**(3), 199–203 (2015).
[9] E.A. Kittlaus, H. Shin, and P.T. Rakich, "Large Brillouin amplification in silicon," Nat. Photonics **10**(7), 463–467 (2016).
[10] R. Pant, C. Poulton, H. MacFarlane, L. Thevenaz, D.Y. Choi, J. Steve, S.J. Madden, B. Luther-Davies, and B.J. Eggleton, "On-chip stimulated brillouin scattering," Opt. Express **19**(9), 8285–8290 (2011).
[11] P. Lei, M. Xu, Y. Bai, Z. Chen, and X. Xie, "Anti-resonant acoustic waveguides enabled tailorable Brillouin scattering on chip," Nat. Commun. 2024 151 **15**(1), 1–8 (2024).
[12] H. Kim, and H. Shin, "Large on-chip Brillouin net amplification in silicon-based nano-photonics," AIP Adv. **9**(12), 125032 (2019).
[13] A. Butsch, M.S. Kang, T.G. Euser, J.R. Koehler, S. Rammler, R. Keding, and P.S.J. Russell, "Optomechanical nonlinearity in dual-nanoweb structure suspended inside capillary fiber," Phys. Rev. Lett. **109**(18), 183904 (2012).
[14] P. Dainese, P.S.J. Russell, N. Joly, J.C. Knight, G.S. Wiederhecker, H.L. Fragnito, V. Laude, and A. Khelif, "Stimulated Brillouin scattering from multi-GHz-guided acoustic phonons in nanostructured photonic crystal fibres," Nat. Phys. **2**(6), 388–392 (2006).
[15] G. Bahl, M. Tomes, F. Marquardt, and T. Carmon, "Observation of spontaneous Brillouin cooling," Nat. Phys. **8**(3), 203–207 (2012).
[16] M.S. Kang, A. Nazarkin, A. Brenn, and P.S.J. Russell, "Tightly trapped acoustic phonons in photonic crystal fibres as highly nonlinear artificial Raman oscillators," Nat. Phys. **5**(4), 276–280 (2009).
[17] Z. Zhu, D.J. Gauthier, and R.W. Boyd, "Stored light in an optical fiber via stimulated brillouin scattering," Science (80-.). **318**(5857), 1748–1750 (2007).
[18] M. Merklein, L. Goulden, M. Kiewiet, Y. Liu, C.K. Lai, D.Y. Choi, S.J. Madden, C.G. Poulton, and B.J. Eggleton, "On-chip quasi-light storage for long optical delays using Brillouin scattering," APL Photonics **9**(5), 56107 (2024).
[19] A. Choudhary, B. Morrison, I. Aryanfar, S. Shahnia, M. Pagani, Y. Liu, K. Vu, S. Madden, D. Marpaung, and B.J. Eggleton, "Advanced Integrated Microwave Signal Processing with Giant On-Chip Brillouin Gain," J. Light. Technol. **35**(4), 846–854 (2017).
[20] W. Zhang, and R.A. Minasian, "Widely tunable single-passband microwave photonic filter based on stimulated Brillouin scattering," IEEE Photonics Technol. Lett. **23**(23), 1775–1777 (2011).
[21] J.C. Beugnot, S. Lebrun, G. Pauliat, H. Maillotte, V. Laude, and T. Sylvestre, "Brillouin light scattering from surface acoustic waves in a subwavelength-diameter optical fibre," Nat. Commun. **5**(1), 1–6 (2014).
[22] W. Xu, A. Iyer, L. Jin, S.Y. Set, and W.H. Renninger, "Strong optomechanical interactions with long-lived fundamental acoustic waves," Optica **10**(2), 206 (2023).
[23] W. Qiu, P.T. Rakich, H. Shin, H. Dong, M. Soljačić, and Z. Wang, "Stimulated Brillouin scattering in nanoscale silicon step-index waveguides: a general framework of selection rules and calculating SBS gain," Opt. Express **21**(25), 31402 (2013).
[24] G.S. Wiederhecker, P. Dainese, and T.P.M. Alegre, "Brillouin optomechanics in nanophotonic structures," APL Photonics **4**(7), 071101 (2019).
[25] C. Wolff, R. Van Laer, M.J. Steel, B.J. Eggleton, and C.G. Poulton, "Brillouin resonance broadening due to

structural variations in nanoscale waveguides," New J. Phys. **18**(2), 025006 (2016).
[26] E. Snitzer, "Cylindrical Dielectric Waveguide Modes," J. Opt. Soc. Am. **51**(5), 491 (1961).
[27] C.K. Ha, K.H. Nam, and M.S. Kang, "Efficient harmonic generation in an adiabatic multimode submicron tapered optical fiber," Commun. Phys. **4**(1), 1–9 (2021).
[28] C. Baker, and M. Rochette, "A generalized heat-brush approach for precise control of the waist profile in fiber tapers," Opt. Mater. Express **1**(6), 1065 (2011).
[29] J.E. Hoffman, S. Ravets, J.A. Grover, P. Solano, P.R. Kordell, J.D. Wong-Campos, L.A. Orozco, and S.L. Rolston, "Ultrahigh transmission optical nanofibers," AIP Adv. **4**(6), 67124 (2014).
[30] W.H. Renninger, R.O. Behunin, and P.T. Rakich, "Guided-wave Brillouin scattering in air," Optica **3**(12), 1316–1319 (2016).
[31] A. Iyer, W. Xu, J.E. Antonio-Lopez, R.A. Correa, and W.H. Renninger, "Ultra-low Brillouin scattering in anti-resonant hollow-core fibers," APL Photonics **5**(9), 096109 (2020).
[32] N. Riesen, and J.D. Love, "Weakly-guiding mode-selective fiber couplers," IEEE J. Quantum Electron. **48**(7), 941–945 (2012).
[33] J.D. Love, and N. Riesen, "Mode-selective couplers for few-mode optical fiber networks," Opt. Lett. **37**(19), 3990 (2012).
[34] G. Agrawal, *Nonlinear Fiber Optics* (Elsevier, 2012).
[35] S. Gertler, N.T. Otterstrom, M. Gehl, A.L. Starbuck, C.M. Dallo, A.T. Pomerene, D.C. Trotter, A.L. Lentine, and P.T. Rakich, "Narrowband microwave-photonic notch filters using Brillouin-based signal transduction in silicon," Nat. Commun. **13**(1), 1–8 (2022).
[36] K.S. Olsson, N. Klimovich, K. An, S. Sullivan, A. Weathers, L. Shi, and X. Li, "Temperature dependence of Brillouin light scattering spectra of acoustic phonons in silicon," Appl. Phys. Lett. **106**(5), (2015).
[37] A. Zadok, E. Zehavi, and A. Bernstein, "Opto-mechanical fiber sensing with optical and acoustic cladding modes," APL Photonics **8**(7), (2023).
[38] R.M. Shelby, M.D. Levenson, and P.W. Bayer, "Guided acoustic-wave Brillouin scattering," Phys. Rev. B **31**(8), 5244–5252 (1985).
[39] J.D. Love, W.M. Henry, W.J. Stewart, R.J. Black, S. Lacroix, and F. Gonthier, "Tapered single-mode fibres and devices Part 1. Adiabaticity criteria," IEE Proceedings. Part J, Optoelectron. **138**(5), 343–354 (1991).
[40] M.C. Frawley, A. Petcu-Colan, V.G. Truong, and S. Nic Chormaic, "Higher order mode propagation in an optical nanofiber," Opt. Commun. **285**(23), 4648–4654 (2012).
[41] R. Nagai, and T. Aoki, "Ultra-low-loss tapered optical fibers with minimal lengths," Opt. Express **22**(23), 28427 (2014).
[42] X. Bao, Y. Dong, D. Zhou, H. Zhang, C. Pang, Z. Hua, and L. Chen, "Opto-mechanical time-domain analysis based on coherent forward stimulated Brillouin scattering probing," Opt. Vol. 7, Issue 2, Pp. 176-184 **7**(2), 176–184 (2020).
[43] Y. Lai, K.Y. Yang, M.-G. Suh, and K.J. Vahala, "Fiber taper characterization by optical backscattering reflectometry," Opt. Express **25**(19), 22312 (2017).
[44] D.M. Chow, Z. Yang, M.A. Soto, and L. Thévenaz, "Distributed forward Brillouin sensor based on local light phase recovery," Nat. Commun. 2018 91 **9**(1), 1–9 (2018).